The Astrophysical Journal, 954:198 (8pp), 2023 September 10 https://doi.org/10.3847/1538-4357/aced93

Metallicities of Classical Cepheids in the Inner Galactic Disk

Noriyuki Matsunaga[1,2], Daisuke Taniguchi[3], Scarlet S. Elgueta[4,5,6,7], Takuji Tsujimoto[3], Junichi Baba[8], Andrew McWilliam[9], Shogo Otsubo[2], Yuki Sarugaku[2], Tomomi Takeuchi[2], Haruki Katoh[2], Satoshi Hamano[3], Yuji Ikeda[2,10], Hideyo Kawakita[2,11], Charlie Hull[9], Rogelio Albarracín[5,6,7], Giuseppe Bono[12,13], and Valentina D'Orazi[12,14]
[1] Department of Astronomy, School of Science, The University of Tokyo, 7-3-1 Hongo, Bunkyo-ku, Tokyo 113-0033, Japan; matsunaga@astron.s.u-tokyo.ac.jp
[2] Laboratory of Infrared High-resolution spectroscopy (LiH), Koyama Astronomical Observatory, Kyoto Sangyo University, Motoyama, Kamigamo, Kita-ku, Kyoto 603-8555, Japan
[3] National Astronomical Observatory of Japan, 2-21-1 Osawa, Mitaka, Tokyo 181-8588, Japan
[4] Instituto de Estudios Astrofísicos, Universidad Diego Portales, Av. Ejército Libertador 441, Santiago, Chile
[5] Instituto de Astrofísica, Pontificia Universidad Católica de Chile, Av. Vicuña Mackenna 4860, 782-0436 Macul, Santiago, Chile
[6] Millenium Nucleus ERIS, Instituto de Estudios Astrofísicos, Universidad Diego Portales, Av. Ejército Libertador 441, Santiago, Chile
[7] Millennium Institute of Astrophysics, Av. Vicuña Mackenna 4860, 782-0436 Macul, Santiago, Chile
[8] Amanogawa Galaxy Astronomy Research Center, Graduate School of Science and Engineering, Kagoshima University, 1-21-35 Korimoto, Kagoshima, Kagoshima 890-0065, Japan
[9] Observatories of the Carnegie Institution for Science, 813 Santa Barbara Street, Pasadena, CA 91101, USA
[10] Photocoding, 460-102 Iwakura-Nakamachi, Sakyo-ku, Kyoto 606-0025, Japan
[11] Department of Astrophysics and Atmospheric Sciences, Faculty of Science, Kyoto Sangyo University, Motoyama, Kamigamo, Kita-ku, Kyoto 603-8555, Japan
[12] Dipartimento di Fisica, Universita di Roma Tor Vergata, via della Ricerca Scientifica 1, I-00133 Roma, Italy
[13] INAF Osservatorio Astronomico di Roma, via Frascati 33, I-00078 Monte Porzio Catone, Italy
[14] INAF Osservatorio Astronomico di Padova, Vicolo dell'Osservatorio 5, I-35122 Padova, Italy
Received 2023 July 18; revised 2023 August 3; accepted 2023 August 4; published 2023 September 7

Abstract

Metallicity gradients refer to the sloped radial profiles of the metallicities of gas and stars and are commonly seen in disk galaxies. A well-defined metallicity gradient of the Galactic disk is observed particularly well with classical Cepheids, which are good stellar tracers thanks to their period–luminosity relation, allowing precise distance estimation and other advantages. However, the measurement of the inner-disk gradient has been impeded by the incompleteness of previous samples of Cepheids and the limitations of optical spectroscopy in observing highly reddened objects. Here we report the metallicities of 16 Cepheids measured with high-resolution spectra in the near-infrared *YJ* bands. These Cepheids are located at 3–5.6 kpc in Galactocentric distance, $R_{\rm GC}$, and reveal the metallicity gradient in this range for the first time. Their metallicities are mostly between 0.1 and 0.3 dex in [Fe/H] and more or less follow the extrapolation of the metallicity gradient found in the outer part, $R_{\rm GC} > 6.5$ kpc. The gradient in the inner disk may be shallower or even flat, but the small sample does not allow the determination of the slope precisely. More extensive spectroscopic observations would also be necessary for studying minor populations, if any, with higher or lower metallicities that were reported in previous literature. In addition, the 3D velocities of our inner-disk Cepheids show a kinematic pattern that indicates noncircular orbits caused by the Galactic bar, which is consistent with the patterns reported in recent studies on high-mass star-forming regions and red giant branch stars.

Unified Astronomy Thesaurus concepts: Cepheid variable stars (218); Metallicity (1031); Milky Way disk (1050); Young disk Cepheid variable stars (1832); Infrared spectroscopy (2285)

1. Introduction

Metallicity gradients have been actively measured in large samples of external galaxies (e.g., Wuyts et al. 2016; Kreckel et al. 2019), and great efforts have also been made in theoretical studies (Bellardini et al. 2022; Tissera et al. 2022). The gradients are shaped by various physical processes, such as gas accretion, star formation, and mass loss through stellar feedback at each position of the disk, as well as the radial migration of stars and gas across the disk, etc. Therefore, understanding the gradients would be a landmark achievement in galactic astronomy.

The most common trend in spiral disks is the negative gradient showing the lower abundance in the outer part, and the same trend is found in the Galaxy. Particularly good tracers of the Galactic gradient are classical Cepheids, which are pulsating stars aged 20–300 Myr and distance indicators following the period–luminosity relation (PLR; Matsunaga et al. 2018). Cepheids show a clear metallicity gradient as tight as ∼0.1 dex, which is even comparable with the measurement errors of the metallicities (Genovali et al. 2014; Luck 2018). However, previous measurements of Cepheids' abundances have been limited in terms of the Galactocentric distance, $R_{\rm GC}$. Luck (2018) provides the largest catalog of abundance measurements of a "classical" sample of more than 400 Cepheids spread over 5–15 kpc in $R_{\rm GC}$, but very little is known about Cepheids in the inner part (<5 kpc) and those in the outer part (>15 kpc).

Cepheids belong to young stellar populations and show a strong concentration in the Galactic disk. Surveys of such variables have been hampered by interstellar extinction, and we have had to wait for the advent of infrared (IR) surveys revealing Cepheids in more extensive parts of the Galaxy. After some dedicated IR surveys of small regions of interest, e.g.,

toward the Galactic center (Matsunaga et al. 2011) and the inner Galactic disk (Tanioka et al. 2017; Inno et al. 2019), large-scale surveys in the near-IR to mid-IR have discovered thousands of new Cepheids spread over a large part of the Galactic disk (Chen et al. 2019; Dékány et al. 2019; Skowron et al. 2019). These "modern" samples enable us to extend our knowledge of the metallicity gradient and, if any, the accompanying substructure, such as the azimuthal variation traced with Cepheids. For example, Trentin et al. (2023) and da Silva et al. (2023) measured the chemical abundances of recently identified Cepheids located beyond 20 kpc in $R_{\rm GC}$. However, such distant Cepheids tend to be affected by high interstellar extinction and require spectroscopic measurements in the IR range instead of optical spectroscopy, which has been used in most previous works.

The targets of this study are Cepheids in the inner disk ($3 < R_{\rm GC} < 5.6$ kpc), and we collected their near-IR spectra to measure the chemical abundances. Many previous studies have suggested that the metallicity gradient gets shallow or flat in the inner disk (Andrievsky et al. 2002, 2016; Bono et al. 2013; Martin et al. 2015; Inno et al. 2019), but almost no Cepheids were located at $R_{\rm GC} < 5$ kpc in the previous samples, as we review in Appendix. The recent large-scale surveys supplemented with IR photometric databases, including time-series measurements, allow us to select a good sample of Cepheids truly located in the inner disk, $3 < R_{\rm GC} \lesssim 5.6$ kpc. Moreover, thanks to the progress in near-IR spectroscopy, in terms of both instrumentation and data analysis, we can use near-IR high-resolution spectra of the inner-disk Cepheids affected by interstellar extinction to measure the chemical abundances precisely.

2. Targets and Observations

2.1. Targets

To make a sample list of Cepheids in the inner disk, we determined the distances to classical Cepheids toward the (southern) Galactic disk and the Galactic center region found by the Optical Gravitational Lensing Experiment (OGLE; Soszyński et al. 2020), using the PLR. We used the photometric data from OGLE, from the Two Micron All Sky Survey (2MASS; Skrutskie et al. 2006), and from the Wide-field Infrared Survey Explorer (WISE; Mainzer et al. 2011, 2014). Combining these photometric data with the PLR, we determined the distance and the foreground extinction of each Cepheid. The same analysis, but for an RR Lyr variable with different PLR, was detailed in Matsunaga et al. (2022). Then we checked that the obtained distances are consistent with the parallax-based distances obtained by Bailer-Jones et al. (2021). This comparison with the geometric distance estimate is useful for confirming that each target is not, e.g., a type II Cepheid, but a classical Cepheid, although the PLR-based distances are more precise at the distances of our targets, $\gtrsim$3 kpc.

Our distance estimates agree with those in Skowron et al. (2019) within ±10%, except for three objects. The differences for Cep015.26+00.28 (=OGLE-BLG-CEP-156) and Cep031.77+00.30 (=OGLE-GD-CEP-1241) are 16% and 12%, respectively, and they are not statistically significant, within 2 σ. In contrast, our distance of Cep327.30−00.39 (=OGLE-GD-CEP-1095) is 33% smaller than the estimate in Skowron et al. (2019), 3.5 kpc versus 4.7 kpc, with a 3 σ significance. This is the most reddened Cepheid among the targets (Table 1), and our estimate $A_V = 18.65$ is significantly larger than $A_V = 12.10$ in Skowron et al. (2019), where $A_K/A_V = 0.078$ from Wang & Chen (2019) is assumed. Skowron et al. (2019) estimated the distances to Cepheids using only the WISE W_1 and W_2 bands, for which the above difference in A_V corresponds to ∼0.25 mag in distance modulus (13% difference in distance). Thus, the difference in estimated A_V explains the difference in distance only partly. Nevertheless, we use our estimate, which is consistent with all six photometric bands of the WISE, 2MASS, and OGLE data sets. Besides, the distance from Skowron et al. (2019) would put this Cepheid in the direction $l = -32.^{\circ}7$ at $R_{\rm GC} = 4.90$ kpc, instead of 5.51 kpc, giving no significant impact on our conclusions below.

To calculate the $R_{\rm GC}$ of our targets, we adopted the distance to the Galactic center, 8.15 kpc, from Reid et al. (2019). Taking other factors, e.g., the light-curve shapes, into account, we selected ∼40 objects that are genuine classical Cepheids located in the inner disk as spectroscopic targets. In the observing run in 2023 June, we observed 16 Cepheids, listed in Table 1. The foreground extinctions, A_V, given in the table indicate that they are highly reddened and IR spectroscopy is required for many of them. Their J-band magnitudes range from 8.5 to 11 mag.

2.2. Observation and Data Reduction

We collected high-resolution spectra of the 16 Cepheids using the WINERED spectrograph attached to the Magellan Clay 6.5 m telescope on 2023 June 6 and 9 (Table 1). WINERED is a near-IR high-resolution spectrograph covering 0.90–1.35 μm (z', Y, and J bands), with a resolution of $R = \lambda/\Delta\lambda = 28{,}000$ with the WIDE mode (Ikeda et al. 2022). The commissioning of WINERED on the Magellan Clay telescope occurred in 2022.

The raw spectral data were reduced with the WINERED Automatic Reduction Pipeline (WARP,[15] version 3.8). In this work, we used spectra without telluric correction and selected absorption lines that were not affected by telluric lines. This reduces the number of absorption lines available for the abundance analysis. Nevertheless, a large fraction of the Y band is almost free from telluric absorption (Smette et al. 2015), and we can find a sufficient number of useful Fe I lines.

2.3. Velocities of Cepheids

We measured the radial velocities of the Cepheids following the method described in Matsunaga et al. (2015). In brief, we searched for the redshift/blueshift with which the observed spectra agree well using the model spectra containing both stellar and telluric lines. The obtained instantaneous velocities with respect to the observer need to be transformed to velocities at the standard frames, such as the heliocentric system, with some correction applied. In addition to the standard corrections, the correction of the pulsation effect is necessary to obtain the barycentric velocities of the Cepheids. For this purpose, we used the OGLE's I-band light curves, assuming that the velocity variation has the same shape as the I-band light variation, but with a different amplitude. We adopted the ratio of the amplitudes from Klagyivik & Szabados (2009), i.e., $A(\mathrm{RV})/A(I) = 78.8$ for $\log P > 1.02$ and 77.1 for $\log P < 1.02$.

[15] https://github.com/SatoshiHamano/WARP/

Table 1
Targets and Observation Log

Name	R.A. (J2000.0)	Decl. (J2000.0)	Period (days)	R_{GC} (kpc)	A_V (mag)	Date (UT)	Time (UT)	Exposures (s)	S/N	Phase (cycle)	ΔV_{pul} (km s^{-1})
Cep319.98+00.03	15:07:01.82	−58:16:56.2	6.64488	5.42	9.78	2023-06-7	02:30	90 × 4	110	0.390	0.9
Cep323.85−00.01	15:31:21.07	−56:14:39.9	17.1131	4.81	10.81	2023-06-10	02:34	300 × 2	110	0.616	−20.2
Cep324.81−00.18	15:37:40.59	−55:49:14.5	9.08820	5.29	8.38	2023-06-7	03:13	60 × 2, 90 × 2	160	0.746	5.4
Cep327.30−00.39	15:52:21.15	−54:27:56.8	36.823	5.51	18.65	2023-06-7	03:35	90 × 6	85	0.642	−18.5
Cep331.10+01.03	16:05:21.14	−50:55:00.2	21.7158	4.66	9.11	2023-06-7	04:35	60 × 4	40	0.715	−21.6
Cep335.09−00.80	16:31:10.68	−49:26:07.1	27.0724	3.49	12.62	2023-06-10	02:54	300 × 2	100	0.515	−11.7
Cep339.16+00.10	16:43:24.63	−45:49:18.6	7.4943	3.92	7.52	2023-06-10	03:10	300 × 2	160	0.248	8.4
Cep345.61−00.38	17:07:47.68	−41:05:47.5	17.2281	3.24	8.49	2023-06-10	03:22	180 × 2	170	0.235	11.8
Cep355.29−00.74	17:36:55.60	−33:19:36.3	8.4876	3.73	6.14	2023-06-10	03:36	180 × 2	160	0.122	10.2
Cep002.04+00.10	17:49:59.77	−27:08:26.4	10.3208	4.78	11.05	2023-06-10	07:25	180 × 2	140	0.914	15.0
Cep014.35+00.34	18:15:19.37	−16:18:34.5	7.1805	4.92	6.93	2023-06-10	08:14	60 × 2	150	0.407	−3.1
Cep015.26+00.28	18:17:20.53	−15:32:42.0	10.2348	5.53	7.84	2023-06-10	08:22	60 × 2	140	0.167	10.2
Cep024.54−01.68	18:42:04.85	−08:13:42.9	23.3672	4.35	4.07	2023-06-10	07:56	150 × 2	180	0.146	17.5
Cep027.93−00.85	18:45:19.75	−04:50:01.8	15.3673	3.84	6.52	2023-06-10	07:36	180 × 2	160	0.206	15.9
Cep028.76−00.43	18:45:20.46	−03:54:29.6	17.6241	4.70	12.22	2023-06-10	07:47	180 × 2	120	0.934	17.6
Cep031.77+00.30	18:48:14.64	−00:53:31.8	40.0109	4.95	14.72	2023-06-10	08:07	180 × 2	100	0.597	−14.7

Table 2
Results: 3D Velocities and Stellar Parameters of Cepheids

Name	V_{helio} (km s^{-1})	V_{LSR} (km s^{-1})	V_R (km s^{-1})	V_{rot} (km s^{-1})	V_Z (km s^{-1})	T_{eff} (K)	log g (dex)	v_{broad} (km s^{-1})	ξ (km s^{-1})	[Fe/H] (dex)
Cep319.98+00.03	−62.8	−62.2	22.1	215.4	3.7	5524	1.70	16.0	3.16	0.04 ± 0.13
Cep323.85−00.01	−91.2	−89.5	7.8	228.6	8.9	4838	1.01	25.0	4.47	-0.06 ± 0.15
Cep324.81−00.18	−36.2	−34.2	1.6	190.8	−0.9	5804	1.73	18.5	4.83	0.14 ± 0.14
Cep327.30−00.39	−68.0	−65.3	6.1	236.8	0.3	5168	0.94	25.0	5.05	0.28 ± 0.13
Cep331.10+01.03	−88.9	−85.0	40.5	209.3	−16.4	4944	0.99	25.0	4.87	0.27 ± 0.19
Cep335.09−00.80	−121.5	−116.7	14.7	217.4	−9.7	4677	0.76	18.5	4.62	0.22 ± 0.16
Cep339.16+00.10	−95.0	−89.0	44.8	193.2	7.4	5657	1.73	14.5	2.88	0.16 ± 0.11
Cep345.61−00.38	−118.4	−110.7	44.0	216.0	−1.4	4996	1.10	16.0	3.65	0.26 ± 0.15
Cep355.29−00.74	−76.4	−66.4	48.5	213.7	−9.8	5744	1.73	16.0	3.78	0.18 ± 0.11
Cep002.04+00.10	14.6	26.1	−22.1	206.6	−14.3	5846	1.71	18.5	4.37	0.26 ± 0.15
Cep014.35+00.34	24.0	37.8	−11.6	208.6	6.0	5498	1.66	14.5	3.19	0.15 ± 0.08
Cep015.26+00.28	8.6	22.6	3.9	227.7	−5.0	5410	1.50	17.0	3.39	0.18 ± 0.14
Cep024.54−01.68	67.2	82.1	4.4	228.1	2.7	5908	1.47	21.5	5.35	0.09 ± 0.17
Cep027.93−00.85	83.0	98.5	−38.8	206.4	9.6	5233	1.27	17.0	2.96	0.30 ± 0.14
Cep028.76−00.43	94.5	110.1	−24.8	251.6	10.7	5842	1.53	25.0	3.43	0.27 ± 0.18
Cep031.77+00.30	94.8	110.7	−29.5	253.9	5.2	4570	0.56	21.5	4.31	0.21 ± 0.17

Such approximate corrections of the pulsation are subject to relatively large errors, ±13 km s^{-1} (Matsunaga et al. 2015), but the corrected velocities allow us to discuss the kinematics of Cepheids in the inner disk. We obtained the heliocentric velocities, V_{helio}, and the velocities with respect to the local standard of rest (LSR), V_{LSR}, as listed in Table 2, using the correction of the pulsation effect, ΔV_{pul}, in Table 1.

The proper motions of our targets are available in Data Release 3 of the Gaia satellite (Gaia Collaboration et al. 2023a). The errors in the proper motions, 0.1–0.2 mas yr^{-1}, correspond to the errors of $\lesssim$5 km s^{-1} at the distances of our Cepheids. We adopted the distance from the Sun to the Galactic center, 8.15 kpc, and the Galactic rotation speed at the solar position, 236 km s^{-1}, from Reid et al. (2019), while the solar velocities to the LSR were taken from Schönrich et al. (2010). Table 2 lists the 3D velocity in the cylindrical Galactocentric frame (V_R, V_{rot}, and V_Z). When positive, V_R, V_{rot}, and V_Z indicate velocities in the outward direction, the Galactic rotation direction, and toward the North Galactic Pole, respectively.

Figure 1 plots various velocities against the Galactic longitude, l. Approximately, they follow the Galactic rotation; in particular, the small V_Z confirm that these objects are classical Cepheids belonging to young stellar populations in the inner Galactic disk. The sequential distribution in the top panel is consistent with the Galactic rotation in the inner disk expected from the commonly used l–v diagram (Reid et al. 2019). However, the V_R show significant noncircular components. The l-dependent systematic motions, including the amplitude of ±40 km s^{-1}, are consistent with the quadrupole pattern caused by the bar detected with red giant branch stars (Bovy et al. 2019; Queiroz et al. 2021; Gaia Collaboration et al. 2023b). Our sample indicates that the same pattern is clearly seen in stars as young as 20–50 Myr, considering that their periods, P, are mostly within 7–30 days (Anderson et al. 2016). A similar systematic motion caused by the bar was also found among high-mass star-forming regions in the Scutum spiral arm by Immer et al. (2019) and Li et al. (2022), whose sample is only on the northern side ($0° < l < 35°$).

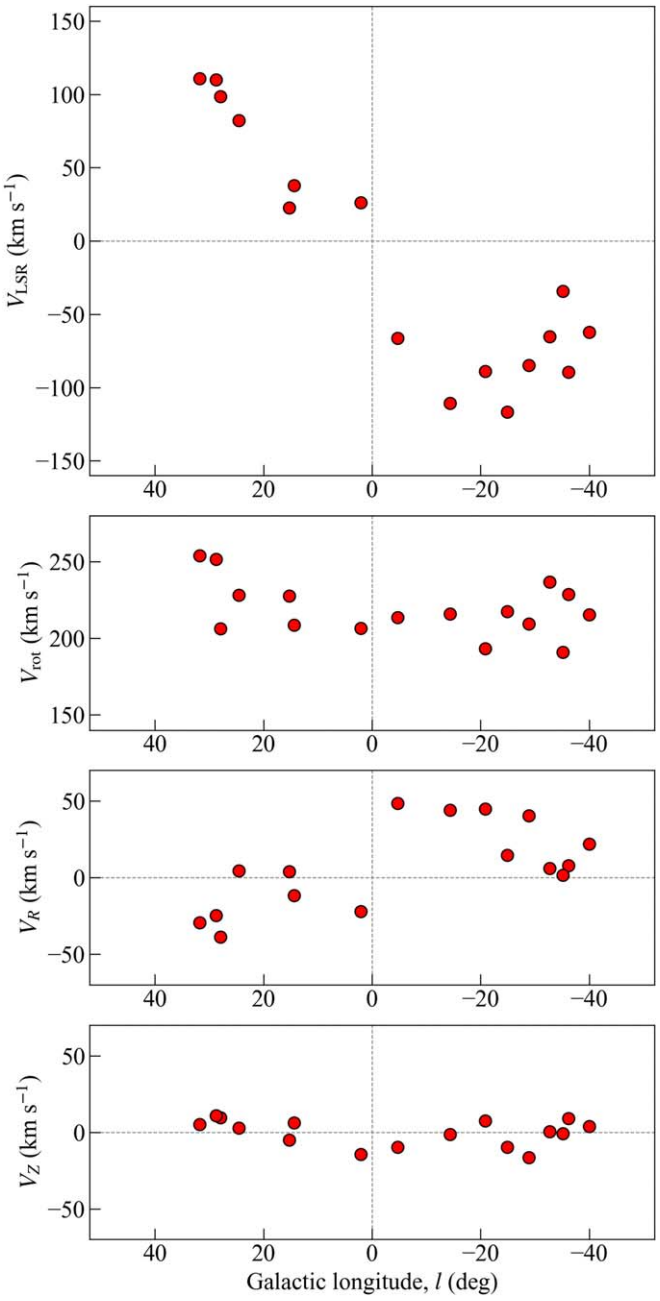

Figure 1. Velocities of Cepheids plotted against the Galactic longitude.

3. Chemical Abundance Analysis

3.1. Stellar Parameters

First, we used the line depth ratio (LDR) method to estimate the effective temperatures ($T_{\rm eff}$) for individual spectra. The method and application to WINERED spectra are presented in Matsunaga et al. (2021) and references therein. Recently, Elgueta (2022) established the LDR relations of 12 Fe I–Fe I pairs that can be used for Cepheids with $4500 < T_{\rm eff} < 6500$ K (see also Elgueta et al. 2023), and we used eight of their relations for which the Fe I lines are unaffected by telluric absorption. The eight pairs worked well for most of our Cepheids, and we obtained $T_{\rm eff}$ in Table 2 with errors $\sim$100 K or smaller. However, the spectra of Cep024.54−01.68 and Cep028.76−00.43 show significantly smaller numbers of absorption lines, clearly indicating high $T_{\rm eff}$, so we could use only five line pairs and the resultant error in $T_{\rm eff}$ is slightly high, $\sim$150 K.

Second, the surface gravity can be estimated with the relation

$$\log g = 6.483 \log(T_{\rm eff}/5800) - 0.775 \log P + 2.475, \quad (1)$$

which was found by Elgueta (2022) for well-known Cepheids taken from Luck (2018). The dispersion of this relation is small, 0.108 dex. Although its $\log g$ scale may have systematic errors present in the measurements by Luck (2018), it enables precise and robust estimates of $\log g$ consistent with their analysis.

Finally, we estimated the broadening widths, $v_{\rm broad}$, of the metallic absorption lines by comparing several Fe I lines in the observed spectra with synthetic spectra with different broadening widths. Our estimates of these three parameters ($T_{\rm eff}$, $\log g$, and $v_{\rm broad}$) are given in Table 2.

3.2. Measurement of Metallicity

The last step of the spectral analysis for this paper is to determine the metallicity ([Fe/H]) and its error, together with the microturbulent velocity (ξ). We selected 30 Fe I lines, mostly in the Y band, unaffected by telluric absorption (see Section 2.2), from the line list with calibrated oscillator strengths ($\log gf$) in Elgueta (2022). The calibration was done based on the WINERED spectra of several Cepheids from Luck (2018), and the $\log gf$ values of the YJ-band Fe I lines were adjusted to give [Fe/H] consistent with the measurements from Luck (2018) with optical high-resolution spectra. We adopted the solar abundance from Asplund et al. (2009), $\log \epsilon_{\odot}({\rm Fe}) = 7.50$, to calculate [Fe/H] here and elsewhere in this paper.

To determine [Fe/H] and ξ simultaneously, we used a similar approach to the ones used in a series of our papers (Kondo et al. 2019; Fukue et al. 2021; Elgueta 2022; Elgueta et al. 2023). First, we estimated the [Fe/H] of each Fe I line as a function of ξ. Then we searched for ξ at which the line-by-line [Fe/H] become independent of the line strength that is represented by the index $X = \log gf - (5040 \times {\rm EP})/(0.86 \times T_{\rm eff})$. We also checked afterward that the line-by-line [Fe/H] show no significant dependence on the excitation potential. We thus obtained the ξ and [Fe/H] of our 16 Cepheids as given in Table 2. The 16 Cepheids have metallicities similar to each other, with a standard deviation of [Fe/H] of 0.096 dex and, on average, significantly higher than solar.

As in Elgueta (2022), we used the OCTOMAN package, developed by one of the authors (D.T.), which determines the abundance together with other free parameters to match the observed spectra with the synthetic spectra. We used the ATLAS9-APOGEE atmosphere models (Mészáros et al. 2012). Including Luck (2018), a significant fraction of the studies measuring the chemical abundances of Cepheids used the atmosphere models of spherical geometry (in particular, MARCS; Gustafsson et al. 2008). However, in the multi-dimensional space of stellar parameters including $T_{\rm eff}$, $\log g$, and [Fe/H], Cepheids are located at around the edge of the grid of the MARCS atmosphere models, and the interpolation of the models often fails during the iterative process of the OCTOMAN tasks. The grid of the MARCS models is sparse at $T_{\rm eff} > 5500$ K, and some grid points miss the models due to a failure in calculation convergence. On the other hand, for relatively massive stars with warmer temperatures, like

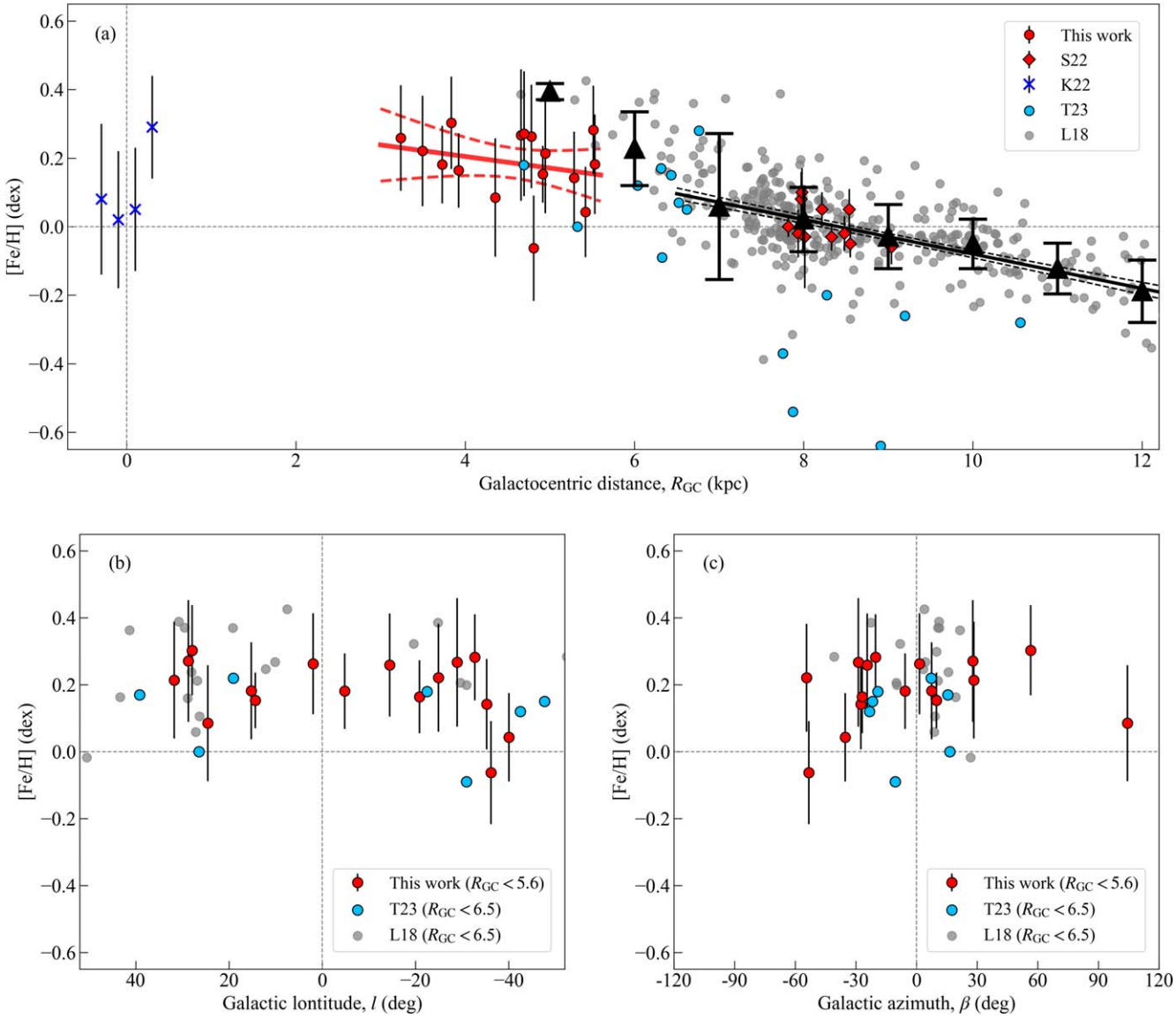

Figure 2. The metallicity distribution of Cepheids plotted against (a) R_{GC}, (b) l, and (c) β. The red circles indicate our results, while the other symbols indicate the results from some relevant papers—Luck (2018) with gray circles, Kovtyukh et al. (2022) with blue crosses, Elgueta (2022) with red diamonds, and Trentin et al. (2023) with blue circles. The error bars for our measurements include the systematic errors, while those for Kovtyukh et al. (2022) and Elgueta (2022) include the standard deviation of line-by-line [Fe/H] only. The black triangles in panel (a) show the averaged metallicity of the Cepheids from Luck (2018) in bins with a width of 1 kpc at each position. The linear regression to the metallicity gradient is indicated by the red line, together with the 90% confidence interval for our Cepheids, while the black counterpart indicates the gradient obtained for the Cepheids from Luck (2018) at $R_{GC} > 6.5$ kpc. In panels (b) and (c), only the objects in the inner disk ($3 < R_{GC} < 6.5$ kpc) are compared.

Cepheids, the spherical effect has been suggested to be within 0.1 dex (Heiter & Eriksson 2006).

During the above estimation of [Fe/H] and ξ, we fixed five parameters of the atmosphere models, i.e., T_{eff}, log g, v_{broad}, [α/Fe], and [C/Fe], of which the last two abundance ratios were assumed to be zero. In contrast, the metallicity [Fe/H] of the atmospheric model changed together with the [Fe/H] being used for synthesizing the Fe I lines, so that the prediction of the line strengths was self-consistent. Then we estimated the systematic errors caused by the uncertainty in the stellar parameters as follows. We evaluated how much the [Fe/H] for reproducing each line absorption would change by differentiating each of the following six parameters by the amount given in parentheses: T_{eff} ($\pm$100 K), log g ($\pm$0.15 dex), ξ ($\pm$0.3 km s^{-1}), [α/Fe] ($\pm$0.3 dex), [C/Fe] ($\pm$0.3 dex), and the model metallicity [Fe/H] ($\pm$0.15 dex). For Cep024.54−01.68 and Cep028.76−00.43, with larger errors in T_{eff}, we used larger offsets, $\pm$150 K. The total systematic errors were finally calculated by combining the above responses to varying the stellar parameters with the standard deviation of the line-by-line abundances in quadrature. Table 2 lists the total errors thus obtained.

4. The Metallicity Gradient

4.1. Our Result

Figure 2 plots the [Fe/H] of the target Cepheids against R_{GC} (upper panel), l (lower left panel), and the Galactic azimuth β (lower right panel). The azimuth β is defined as zero toward the Sun and increasing in the direction of Galactic rotation,

following the definition in Reid et al. (2019), but in degrees. The lower panels include Cepheids at $R_{GC} < 6.5$ kpc, while the upper panel includes those located over a large range of R_{GC}. Apparently, we found no significant azimuthal variation, and thus we focus on the metallicity gradient below.

We obtained the linear regression of the metallicity gradient,

$$[Fe/H] = -0.034(\pm 0.035)R_{GC} + 0.340(\pm 0.161), \quad (2)$$

with a residual scatter of 0.10 dex with the 16 Cepheids. For comparison, we also made a linear regression to the Cepheids at $6.5 < R_{GC} < 15$ kpc from Luck (2018), obtaining

$$[Fe/H] = -0.050(\pm 0.003)R_{GC} + 0.423(\pm 0.029), \quad (3)$$

with a residual scatter of 0.12 dex. Roughly speaking, the 16 Cepheids in this study have the metallicities expected from the extrapolation of the metallicity gradient found in the outer disk ($R_{GC} > 6.5$ kpc). The current result is statistically consistent with a very simple scenario of the gradients of Equations (2) and (3) being connected as a single linear relation. With the current small sample, however, we cannot reject different scenarios. Our 16 Cepheids give a Pearson's correlation coefficient, $r = -0.25$, between R_{GC} and [Fe/H] with a moderate p value, 0.35, leaving the possibility of the null hypothesis, i.e., that the gradient may be flat in the inner disk. While we would need a larger sample to discuss the metallicity gradient in the inner disk in more detail, our sample has already illustrated that, at least, the main group of Cepheids in the inner disk ($R_{GC} < 5.6$ kpc) have metallicities of 0.1–0.3 dex. This raises a few important questions concerning the global metallicity distribution of the Galactic disk, which we discuss in the following subsections.

4.2. Connection with Cepheids in the Galactic Center?

In Figure 2, four Cepheids from Kovtyukh et al. (2022) are located in the Galactic center region. As discussed by Matsunaga et al. (2011, 2015), they are located within the Nuclear Stellar Disk (Launhardt et al. 2002), with a radius of 200–300 pc, but the line-of-sight locations have not been determined. To separate the markers in Figure 2, they are plotted at around $R_{GC} = 0$, but with artificial horizontal offsets added. Although the precision in [Fe/H] is not high, Kovtyukh et al. (2022) concluded that the metallicities of these central Cepheids are close to solar (see also Kovtyukh et al. 2019), but are potentially outliers having slightly higher [Fe/H]. It is tempting to combine these Cepheids with our sample at $3 < R_{GC} < 5.6$ kpc to discuss whether the metallicity gradient is flat or slightly positive (i.e., the [Fe/H] being lower at $R_{GC} < 300$ pc). However, Matsunaga et al. (2016) found that there is a little population of Cepheids in the intermediate range ($0.3 < R_{GC} < 3$ kpc), where star formation may be suppressed by the bar, as seen in other barred galaxies (Maeda et al. 2023). It is totally unknown what connection, if any, we should expect between the two groups of Cepheids in terms of chemical evolution.

4.3. Connection with Super-metal-rich Cepheids in the Inner Disk?

There are several Cepheids with [Fe/H] > 0.35 dex in the catalog of Luck (2018). The trend of the averaged metallicity as a function of R_{GC}, indicated by the black triangle in Figure 2, also shows an upturn at $R_{GC} \lesssim 6.5$ kpc. The presence of such metal-rich Cepheids in the inner disk has also been reported in other papers (Luck & Lambert 2011; Genovali et al. 2013, 2014). If such super-metal-rich Cepheids are confirmed, they would suggest either a bump of the metallicity gradient at $5.6 \lesssim R_{GC} \lesssim 6.5$ kpc or a chemical inhomogeneity that forms stars more metal-rich than the ambient coeval stellar population.

4.4. Connection with Metal-poor Red Supergiant Clusters Near the Bar End?

An intriguing feature of the metallicity distribution in the inner disk is the presence of metal-poor young stars discovered by Davies et al. (2009). They reported that two red supergiant clusters at around $R_{GC} = 3.5$ kpc in the Scutum constellation are significantly low-metal, $[Fe/H] \simeq -0.2$ dex, and they suggested such unexpected low metallicities could result from irregular star formation at around the bar end region. Similar results have been reported for red supergiant clusters near the bar end region by other authors (Origlia et al. 2019 and references therein). Our result indicates that, at least, the dominant population of young stars in the inner disk is more metal-rich than solar, except for Cep323.85−00.01, with $[Fe/H] = -0.06 \pm 0.15$ dex, which is far from the bar end at $\beta = 25°$–$30°$ (Wegg & Gerhard 2013).

5. Summary

We have measured the [Fe/H] of Cepheids located at $3 < R_{GC} < 5.6$ kpc. There were only a couple of Cepheids with metallicity measured in such an inner part of the Galactic disk (Appendix). Therefore, our sample of 16 Cepheids is the first to show the metallicity distribution in this very inner disk in a systematic way. Their [Fe/H] values, mostly within 0.1–0.3 dex, are consistent with the extrapolation of the metallicity gradient found in the outer part ($R_{GC} > 6.5$ kpc). In addition, they are distributed over an extensive range of the Galactic azimuth, and we found no evidence of azimuthal variation. The homogeneity among our sample suggests that the chemical evolution in the inner disk is uniform at the level of ±0.1 dex, although studies with larger samples should follow in order to discuss this point. In particular, the inhomogeneity discussed in several papers (see Sections 4.3 and 4.4) needs to be confirmed (or rejected) with a larger sample.

Acknowledgments

This paper is based on WINERED data gathered with the 6.5 m Magellan Clay Telescope located at Las Campanas Observatory, Chile. It is a great pleasure to thank the staff of Las Campanas Observatory for their support during the WINERED's installation and observations. WINERED was developed by the University of Tokyo and the Laboratory of Infrared High-resolution Spectroscopy, Kyoto Sangyo University, under the financial support of KAKENHI (Nos. 16684001, 20340042, and 21840052) and the MEXT Supported Program for the Strategic Research Foundation at Private Universities (Nos. S0801061 and S1411028). The observing run in 2023 June was partly supported by KAKENHI (grant No. 18H01248) and JSPS Bilateral Program Number JPJSBP120239909. D.T. acknowledges financial support from the JSPS Research Fellowship for Young

Scientists and the accompanying JSPS KAKENHI grant No. 23KJ2149.

Facility: Magellan:Clay (WINERED).

Software: astropy (Astropy Collaboration et al. 2013, 2018), MOOG (Sneden et al. 2012), OCTOMAN (D. Taniguchi et al. 2023, in preparation), WARP (S. Hamano et al. 2023, in preparation).

Appendix
Review of the Inner-disk Cepheids in Previous Works

Here we review the Cepheids in the inner disk that have been considered by previous studies to discuss the metallicity distribution in the inner disk. Two stars, SU Cas and ASAS 181024−2049.6, were suggested to be Cepheids located at $R_{\rm GC}$ as small as 2.5–3 kpc (Martin et al. 2015; Andrievsky et al. 2016). However, the parallax-based distances in Bailer-Jones et al. (2021) indicate that these stars are within 3 kpc of the Sun, and thus their $R_{\rm GC}$ are not smaller than 5 kpc (see also Kovtyukh et al. 2022). Note that the PLR-based distances are accurate only if the classification as classical Cepheids is correct. Misclassification would lead to totally wrong distances, while the parallax-based distances are independent of the variability types.

Among the Cepheids included in the catalog of Luck (2018), BC Aql and V340 Ara have $R_{\rm GC}$ smaller than 5 kpc, but BC Aql is a foreground object according to Bailer-Jones et al. (2021). In contrast, the parallax-based distance to V340 Ara, 4.3 ± 0.4 kpc, supports this star being within 5 kpc of the Galactic center, $R_{\rm GC} \simeq 4.6$ kpc. Accepting that it is a classical Cepheid in the inner disk, V340 Ara is a very interesting target, considering its high metallicity, [Fe/H] = +0.44 dex, and large distance from the Galactic disk, ∼280 pc. For $5 < R_{\rm GC} < 6.5$ kpc, Luck (2018) lists five metal-rich Cepheids with [Fe/H] > 0.35 dex: UZ Sct, AV Sgr, V526 Aql, DV Ser, and AA Ser. Bailer-Jones et al. (2021) support their positions in the inner disk within the uncertainty, but the parallax-based distance to DV Ser suggests that this Cepheid may be even closer to the center, $R_{\rm GC} \simeq 4.2$ kpc.

In addition, there are two Cepheids located at $R_{\rm GC} < 5.6$ kpc among the dozens of Cepheids observed by Trentin et al. (2023), ASAS J164120−4739.6 ($R_{\rm GC} = 4.70$ kpc) and OGLE-GD-CEP-1210 ($R_{\rm GC} = 5.33$ kpc), but with lower [Fe/H], 0.18 and 0.00 dex, respectively. Inno et al. (2019) measured [Fe/H] with near-IR medium-resolution spectra ($R \sim 3000$) for three Cepheids with $5 < R_{\rm GC} < 6$ kpc, in addition to two others with $R_{\rm GC}$ around 7 kpc. They report one of the three inner-disk Cepheids to have a metallicity lower than solar, [Fe/H] ≃ −0.05.

In summary, according to some previous studies, there are some inner-disk Cepheids with metallicities higher ([Fe/H] $\gtrsim$ 0.35 dex) or lower ([Fe/H] $\lesssim$ 0 dex), not following the main trend that we have discovered in this paper (Section 4). The nature of such Cepheids will be an interesting subject of study in the future.

ORCID iDs

Daisuke Taniguchi https://orcid.org/0000-0002-2861-4069
Scarlet S. Elgueta https://orcid.org/0000-0001-5642-2569
Takuji Tsujimoto https://orcid.org/0000-0002-9397-3658
Junichi Baba https://orcid.org/0000-0002-2154-8740
Satoshi Hamano https://orcid.org/0000-0002-6505-3395
Yuji Ikeda https://orcid.org/0000-0003-2380-8582
Hideyo Kawakita https://orcid.org/0000-0003-2011-9159
Giuseppe Bono https://orcid.org/0000-0002-4896-8841
Valentina D'Orazi https://orcid.org/0000-0002-2662-3762

References

Anderson, R. I., Saio, H., Ekström, S., Georgy, C., & Meynet, G. 2016, A&A, 591, A8
Andrievsky, S. M., Bersier, D., Kovtyukh, V. V., et al. 2002, A&A, 384, 140
Andrievsky, S. M., Martin, R. P., Kovtyukh, V. V., Korotin, S. A., & Lépine, J. R. D. 2016, MNRAS, 461, 4256
Asplund, M., Grevesse, N., Sauval, A. J., & Scott, P. 2009, ARA&A, 47, 481
Astropy Collaboration, Price-Whelan, A. M., Sipőcz, B. M., et al. 2018, AJ, 156, 123
Astropy Collaboration, Robitaille, T. P., Tollerud, E. J., et al. 2013, A&A, 558, A33
Bailer-Jones, C. A. L., Rybizki, J., Fouesneau, M., Demleitner, M., & Andrae, R. 2021, AJ, 161, 147
Bellardini, M. A., Wetzel, A., Loebman, S. R., & Bailin, J. 2022, MNRAS, 514, 4270
Bono, G., Matsunaga, N., Inno, L., Lagioia, E. P., & Genovali, K. 2013, in Cosmic Rays in Star-Forming Environments, Astrophysics and Space Science Proceedings, ed. D. F. Torres & O. Reimer, Vol. 34 (Berlin: Springer), 115
Bovy, J., Leung, H. W., Hunt, J. A. S., et al. 2019, MNRAS, 490, 4740
Chen, X., Wang, S., Deng, L., et al. 2019, NatAs, 3, 320
da Silva, R., D'Orazi, V., Palla, M., et al. 2023, arXiv:2308.01928
Davies, B., Origlia, L., Kudritzki, R.-P., et al. 2009, ApJ, 696, 2014
Dékány, I., Hajdu, G., Grebel, E. K., & Catelan, M. 2019, ApJ, 883, 58
Elgueta, S. S. 2022, PhD thesis, Univ. Tokyo doi:10.5281/zenodo.8267162
Elgueta, S. S., Matsunaga, N., Jian, M., et al. 2023, arXiv:2307.00158
Fukue, K., Matsunaga, N., Kondo, S., et al. 2021, ApJ, 913, 62
Gaia Collaboration, Drimmel, R., Romero-Gómez, M., et al. 2023b, A&A, 674, A37
Gaia Collaboration, Vallenari, A., Brown, A. G. A., et al. 2023a, A&A, 674, A1
Genovali, K., Lemasle, B., Bono, G., et al. 2013, A&A, 554, A132
Genovali, K., Lemasle, B., Bono, G., et al. 2014, A&A, 566, A37
Gustafsson, B., Edvardsson, B., Eriksson, K., et al. 2008, A&A, 486, 951
Heiter, U., & Eriksson, K. 2006, A&A, 452, 1039
Ikeda, Y., Kondo, S., Otsubo, S., et al. 2022, PASP, 134, 015004
Immer, K., Li, J., Quiroga-Nuñez, L. H., et al. 2019, A&A, 632, A123
Inno, L., Urbaneja, M. A., Matsunaga, N., et al. 2019, MNRAS, 482, 83
Klagyivik, P., & Szabados, L. 2009, A&A, 504, 959
Kondo, S., Fukue, K., Matsunaga, N., et al. 2019, ApJ, 875, 129
Kovtyukh, V. V., Andrievsky, S. M., Martin, R. P., et al. 2019, MNRAS, 489, 2254
Kovtyukh, V. V., Korotin, S. A., Andrievsky, S. M., Matsunaga, N., & Fukue, K. 2022, MNRAS, 516, 4269
Kreckel, K., Ho, I. T., Blanc, G. A., et al. 2019, ApJ, 887, 80
Launhardt, R., Zylka, R., & Mezger, P. G. 2002, A&A, 384, 112
Li, J. J., Immer, K., Reid, M. J., et al. 2022, ApJS, 262, 42
Luck, R. E. 2018, AJ, 156, 171
Luck, R. E., & Lambert, D. L. 2011, AJ, 142, 136
Maeda, F., Egusa, F., Ohta, K., Fujimoto, Y., & Habe, A. 2023, ApJ, 943, 7
Mainzer, A., Bauer, J., Cutri, R. M., et al. 2014, ApJ, 792, 30
Mainzer, A., Bauer, J., Grav, T., et al. 2011, ApJ, 731, 53
Martin, R. P., Andrievsky, S. M., Kovtyukh, V. V., et al. 2015, MNRAS, 449, 4071
Matsunaga, N., Bono, G., Chen, X., et al. 2018, SSRv, 214, 74
Matsunaga, N., Feast, M. W., Bono, G., et al. 2016, MNRAS, 462, 414
Matsunaga, N., Fukue, K., Yamamoto, R., et al. 2015, ApJ, 799, 46
Matsunaga, N., Itane, A., Hattori, K., et al. 2022, ApJ, 925, 10
Matsunaga, N., Jian, M., Taniguchi, D., & Elgueta, S. S. 2021, MNRAS, 506, 1031
Matsunaga, N., Kawadu, T., Nishiyama, S., et al. 2011, Natur, 477, 188
Mészáros, S., Allende Prieto, C., Edvardsson, B., et al. 2012, AJ, 144, 120
Origlia, L., Dalessandro, E., Sanna, N., et al. 2019, A&A, 629, A117
Queiroz, A. B. A., Chiappini, C., Perez-Villegas, A., et al. 2021, A&A, 656, A156
Reid, M. J., Menten, K. M., Brunthaler, A., et al. 2019, ApJ, 885, 131
Schönrich, R., Binney, J., & Dehnen, W. 2010, MNRAS, 403, 1829
Skowron, D. M., Skowron, J., Mróz, P., et al. 2019, Sci, 365, 478
Skrutskie, M. F., Cutri, R. M., Stiening, R., et al. 2006, AJ, 131, 1163

Smette, A., Sana, H., Noll, S., et al. 2015, A&A, 576, A77
Sneden, C., Bean, J., Ivans, I., Lucatello, S., & Sobeck, J. 2012, MOOG: LTE Line Analysis and Spectrum Synthesis, Astrophysics Source Code Library ascl:1202.009
Soszyński, I., Udalski, A., Szymański, M. K., et al. 2020, AcA, 70, 101
Tanioka, S., Matsunaga, N., Fukue, K., et al. 2017, ApJ, 842, 104
Tissera, P. B., Rosas-Guevara, Y., Sillero, E., et al. 2022, MNRAS, 511, 1667
Trentin, E., Ripepi, V., Catanzaro, G., et al. 2023, MNRAS, 519, 2331
Wang, S., & Chen, X. 2019, ApJ, 877, 116
Wegg, C., & Gerhard, O. 2013, MNRAS, 435, 1874
Wuyts, E., Wisnioski, E., Fossati, M., et al. 2016, ApJ, 827, 74